Energy and Exergy Analyses of a Solar-based Multi-generation Energy Plant Integrated with Heat Recovery System and Thermal Energy Storage

Shayan Sadeghi[1], Samane Ghandehariun[1], Behnaz Rezaie[2]

[1]Sustainable Energy Research Group (SERG), School of Mechanical Engineering, Iran University of Science and Technology, Tehran, Iran

[2]Applied Energy Research Laboratory (AERL), Department of Mechanical Engineering, College of Engineering, University of Idaho, 875 Perimeter Dr., Moscow, ID 83844-0902, USA

Abstract

An innovative multigeneration energy system driven by solar energy is proposed in this paper. The integrated model produces electricity, hydrogen, oxygen, and steam for heating purposes. The energy system comprises of pressurized cavity based solar power tower, latent thermal energy storage (TES) unit, unfired gas turbine (GT) unit, regenerative steam Rankine cycle (SRC), copper-chlorine (Cu-Cl) thermochemical cycle, and heat recovery units. By utilization of a high temperature ternary eutectic phase change material (PCM), a dynamic model is developed to deal with the intermittency of the solar energy. Using energy and exergy approaches, the proposed system is investigated to assess exergy destruction rates and the overall system performance. A parametric study is performed to investigate the influence of design parameters such as number of heliostats, pressure ratio of GT, and temperatures of reactions on the system performance. The results showed that the energy system produces electricity, steam, hydrogen, and oxygen at a rate of 41.9 MW, 12.6 kg/s, 0.19 kg/s, and 0.76 kg/s, respectively. Energy and exergy efficiencies of the integrated system are found to be 49.9%, and 44.9%, respectively.

Keywords
Thermal Energy Storage; Multigeneration System; Thermochemical Cycle; Heat Recovery; Phase Change Material.

Nomenclature		ph	Physical
C_p^o	Specific heat (J/mol.k)	pp	Pinch point
D_p	Depletion number	th	Thermal

$\dot{E}x$	Exergy (W)	turb	Turbine
$\dot{m}$	Mass flow rate (kg/s)	Greek symbols	
$\dot{Q}$	Heat transfer rate (W)	η_I	Energy efficiency
$\dot{W}$	Power (W)	η_{II}	Exergy efficiency
A	Area (m2)	Δ	Difference
ex	Specific exergy (kJ/kg)	Abbreviations	
h	Specific enthalpy (kJ/kg)	AC	Air compressor
P	Pressure (kPa)	CFWH	Close feedwater heater
s	Entropy (J/kg.K)	Cu-Cl	Copper Chlorine
T	Temperature (K)	DNI	Direct normal irradiance
V	Volume (m3)	GT	Gas turbine
Subscripts		HRSG	Heat recovery steam generator
ch	Chemical	HX	Heat exchanger
Cond	Condenser	LHV	Lower heating value
D	Destruction	OFWH	Open feedwater heater
Elec	Electrolyzer	PCM	Phase change material
ex	Exergy	SI	Sustainability index
i	Inlet	SRC	Steam Rankine cycle

L	Loss	ST	Steam turbine
o	Dead state	TES	Thermal energy storage
P	Pump		

1. Introduction

Total energy consumption of the world is growing 3.2% annually [1]. Additionally, with the deterioration of natural resources, it is necessary to use more sustainable energy sources, manage the energy consumption/production more effectively, and use more efficient energy systems [2]. Using renewable energies such as solar or wind energies is important to achieve sustainability goals. Energy storage systems are also required due to intermittency of renewable energy sources [3]. Multigeneration systems which are capable to produce more than one product should be considered to improve the overall performance [4-6].

Pure oxygen is used in industry, medical, space, and marine applications [7]. It is currently used in respiratory devices in hospitals, life support in the space or underwater conditions, and even in industry to produce steel from iron ore [7,8]. Additionally, hydrogen which is a carbon-free energy carrier with high energy density can be of great use for energy management purposes [9]. It is an important substance which can be used as a chemical agent in chemical plants such as refineries to produce high quality fuels such as diesel and gasoline, and also, in petrochemical plants to produce ammonia, methanol, and other chemicals [10].

Currently, hydrogen is mostly produced from fossil fuels. Over 95% of the current hydrogen demand in the world is produced from natural gas and coal, and less than 5% is produced through water electrolysis [11]. Therefore, it is required to investigate more sustainable methods for large-scale hydrogen production. There are few methods in which water splitting processes are used to dissociate water molecules into hydrogen and oxygen

[12]. These methods include thermochemical cycles, photo-electrochemical cells, and electrolysis [12-14]. Thermochemical water splitting is one of the most promising methods for sustainable hydrogen production. A thermochemical cycle decomposes water into hydrogen and oxygen through a series of chemical reactions. All of the chemical compounds produced in the cycle, are used within the cycle. Therefore, the net outputs are only oxygen and hydrogen [15,16]. Some of the thermochemical cycles require thermal energy, and some others, called hybrid cycles, need both thermal energy and electricity [17].

Among over hundreds of different thermochemical cycles presented in the literature, Sulfur-Iodine (S-I) and Copper-Chlorine (Cu-Cl) are known as the most promising thermochemical cycles for hydrogen production [12,13,17]. Heat is required at the maximum temperature of around 900 and 500 ℃ for the S-I and Cu-Cl cycle, respectively [18,19]. A comparative analysis between S-I and CuCl cycle was carried out by Wang et al. [20]. It was shown that the Cu-Cl cycle is more suitable for integration with various renewable energy sources [20].

Due to high temperature requirement of the thermochemical cycles, limited sources of energy are available for integration. Solar energy as one of the most abundant and available renewable energy resources is a good candidate for integration with the Cu-Cl cycle [21,22]. However, due to its intermittency, for a continuous operation of the plant, TES systems should be utilized to store the solar energy during the sunny hours and recover it during cloudy hours or nights. Molten salts, as sensible energy storage materials, are usually used as the TES media in the solar plants [23]. However, considering high costs, limited operating temperature, and large required volumes of the molten salts, PCM can be considered as alternative TES media in the solar plants [24,25].

Some studies explored solar cogeneration/multigeneration systems for producing various outputs especially oxygen and hydrogen. Coupling of a solar system with a five-step Cu-Cl thermochemical cycle was investigated [26]. Solar salt which is a binary mixture of KNO_3

and $NaNO_3$ was selected as the thermal energy storage medium and a thermal efficiency of 49% was reported [26]. A four-step Cu-Cl cycle integrated with a solar parabolic trough collector system was proposed for Algeria. Energy and exergy efficiencies of the Cu-Cl cycle were reported as 48.14% and 92.25%, respectively [27]. In another study, three different types of hydrogen production systems including an ocean thermal powered water electrolysis system, solar Cu-Cl cycle and wind powered water electrolysis system were investigated and compared. It was concluded that the solar Cu-Cl cycle has the highest energy efficiency which is 32.7% [28]. An integrated solar powered Cu-Cl cycle coupled with a hydrogen compression unit was proposed and investigated in another study. The overall energy efficiency of the system was 12.6% [29]. Thermodynamic performance of multigeneration which produced potable water, hydrogen, power, and heating-cooling based on solar energy was investigated in another study. The system utilized solar power tower with Brayton cycle and electrolysis. However, no TES system was considered for continuous operation of the system. The overall system energy and exergy efficiencies were reported as 78.93%, and 47.56%, respectively [30]. In another study, a multigeneration system was investigated which used parabolic solar dish collector to produce electrolytic hydrogen, cooling-heating, and power. Molten salt was considered for sensible TES. The energy and exergy efficiencies of this system were reported as 48.19% and 43.57%, respectively [31]. A hybrid system based on solar and biomass energies were investigated to produce hot water, cooling, hydrogen, and power. A four-step Cu-Cl cycle was used to produce the hydrogen. The energy and exergy efficiencies of the system were evaluated as 29.9% and 31.5%, respectively [32].

Past studies used conventional molten salts as the TES media of their solar subsystems [28,29,31,32]. Also, molten salt was used to produce steam which served as a heat transfer fluid to provide the required heat to the reactors and heat exchangers [28,29,32]. The operating temperature of the molten salt ranges from 290 to 565 ℃ [33] which limits the hydrogen production yield of the plant. Also, the integrated systems were dependent on the grid electricity for the electrolysis step [26-28]. In this study, a novel solar multigeneration system with thermochemical cycle is proposed for sustainable production of oxygen, hydrogen, power, and steam for heating purposes. This energy system does not rely on the external electricity source. Also, air is used as the heat transfer fluid in the plant. The proposed multigeneration system includes a solar heliostat field, pressurized cavity receiver, PCM tank, unfired gas turbine cycle, four-step Cu-Cl cycle, heat recovery steam generator unit and regenerative Rankine cycle. The TES material selected for this study is an eutectic mixture of CaF_2(49)-$CaSO_4$(41.4)-$CaMoO_4$(9.6) fluoride salt with melting temperature of 943 ℃ and fusion enthalpy of 237 kJ/kg [34].

Main objectives of this study are to conduct energy and exergy analyses for the proposed solar multigeneration energy plant to assess the overall system and subsystems performance, and finding the exergy destruction of various components, and also, to compare with the previous studies in the literature. Exergy analysis is a useful tool which can help the design engineers identify the source, type, and amount of lost availability in the system which are caused by irreversibility. Therefore, it is possible to achieve higher efficiencies which result in improving the sustainability. The effects of varying input parameters on the overall energysystem performance are also investigated in this study. The results provide insight for design engineers to determine the major input influencers on the energy system performance.

2. System Description

The schematic of the proposed integrated solar-based hydrogen production plant is shown in Fig. 1. The outputs of the proposed energy system in this study are hydrogen, oxygen, electricity, and steam for heating purposes. The proposed energy system comprises of five subsystems including solar heliostat field and receiver, unfired gas turbine cycle with PCM, four-step cu-cl cycle, regenerative steam Rankine cycle, and heat recovery unit. The air is pressurized by the compressor of the unfired gas turbine unit at state 21 and goes to the pressurized cavity receiver tower. Meanwhile, solar radiations are reflected by the heliostat mirrors to top of the receiver tower to heat up the air. The heated air at state 23 passes through the PCM unit. When the solar radiations are high, the PCM begins to charge up and when the solar radiations are low the PCM discharges. The air then goes through the gas turbine unit in which electricity is generated. The low-pressure air at the exit of the gas turbine unit at state 25 returns to the PCM unit to get heated again. It is because the required temperature for the Cu-Cl cycle is about 530 ℃, and therefore, the temperature of air leaving the PCM unit at state 26 has to be higher than 530 ℃. For the base case, the temperature at state 26 is 600 ℃. Afterwards, the hot air splits into three streams to supply the required heat for the various heat exchangers, reactors, and steam generators in Cu-Cl and Rankine cycles. The air exiting the heat exchangers at states 31, 32, and 33 are used in a heat recovery steam generator unit to produce steam for heating purposes.

Four-step Cu-Cl cycle considered here includes hydrolysis, thermolysis, drying, and electrolysis steps. The first step is the hydrolysis in which water and cupric chloride ($CuCl_2$) react to produce copper oxychloride (Cu_2OCl_2) and hydrogen chloride (HCl) gas at 375-400 ℃ [35]:

$$2CuCl_2(s) + H_2O(g) \rightarrow Cu_2OCl_2(s) + 2HCl(g) \quad (1)$$

Second step is thermolysis in which decomposition of copper oxychloride occurs at high temperatures of 500-530 ℃. The products of this step are oxygen and cuprous chloride (CuCl) [35]:

$$Cu_2OCl_2(s) \rightarrow \frac{1}{2}O_2(g) + 2CuCl(l) \quad (2)$$

The third step is drying of aqueous cupric chloride which occurs at temperatures ranging from 30 to 80 ℃ [35]:

$$CuCl_2(aq) \rightarrow CuCl_2(s) \tag{3}$$

The last step is electrolysis in which hydrogen gas and cupric chloride are produced from the electrochemical reaction of aqueous HCl and CuCl at around 25 ℃ [35]:

$$2CuCl(aq) + 2HCl(aq) \rightarrow H_2(g) + 2CuCl_2(aq) \tag{4}$$

Heat is recovered from the oxygen and molten CuCl leaving the thermolysis reactor at about 530 ℃, and also the HCl leaving the hydrolysis reactor at about 400 ℃. The recovered heat is used to heat up $CuCl_2$ and copper oxychloride, to produce steam, and also to preheat the Rankine cycle's working fluid. Four heat exchangers are used in the Rankine cycle to produce superheated steam. HX9 and HX10 are the preheaters, HX11 is the evaporator, and HX12 is the superheater. Open and closed feedwater heaters use extracted steam at states 52 and 53 to improve the performance of the SRC. The required electricity of the Cu-Cl cycle's electrolyzer is supplied from the produced power of the GT cycle. Additionally, the excess electricity of the GT, and also, the SRC are exported to the electrical grid.

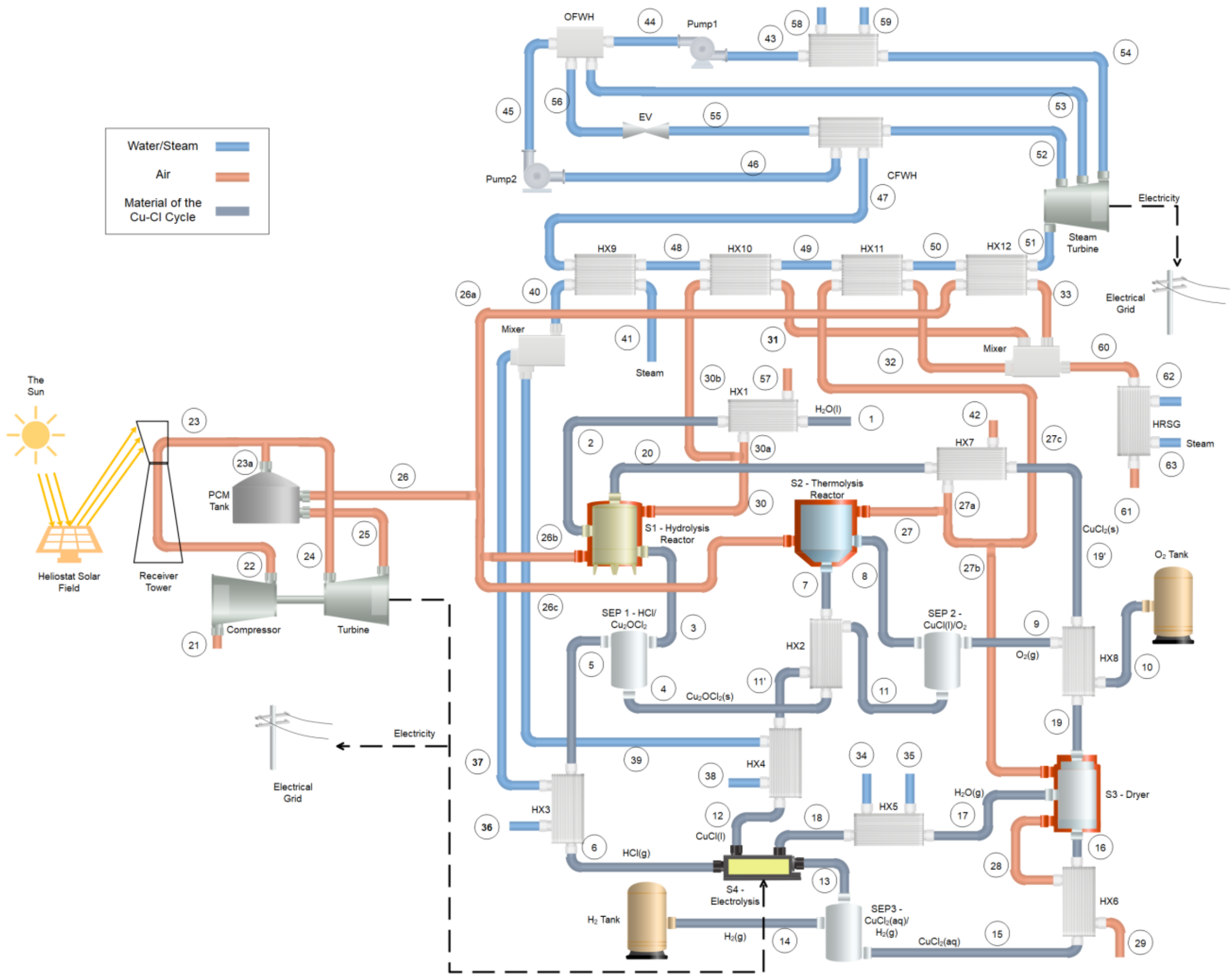

Figure 1 Schematic of the integrated solar-based multigeneration energy plant

3. Methodology

Energy and mass conversions are expressed as follows [36]:

$$\dot{Q} - \dot{W} = \sum(\dot{m}h)_i - \sum(\dot{m}h)_e \tag{5}$$

$$\sum \dot{m}_i - \sum \dot{m}_e = 0 \tag{6}$$

And exergy balance is developed as [36]:

$$\dot{Ex}_d = \dot{Ex}_Q - \dot{Ex}_W + \sum(\dot{m}ex)_i - \sum(\dot{m}ex)_e \quad (7)$$

where, $\dot{Ex}$, $\dot{W}$, $\dot{Q}$, and $\dot{m}$ denote rate of exergy, work, heat, and mass, respectively. Also, ex and h are the specific exergy and enthalpy, respectively. Other terms are calculated from the equations (8) to (11) [36]:

$$\dot{Ex}_Q = (1 - \frac{T_0}{T_i})\dot{Q}_l \quad (8)$$

$$\dot{Ex}_W = \dot{W} \quad (9)$$

$$ex = ex_{ph} + ex_{ch} \quad (10)$$

$$ex_{ph} = (h_i - h_o) - T_o(s_i - s_o) \quad (11)$$

Here, ex_{ch} and ex_{ph} represent chemical and physical specific exergy, respectively. Temperature and pressure of reference environment is considered as 25 ℃ and 101 kPa.

To relate between the environment impacts and exergy, sustainability index is defined as follows [37]:

$$SI = \frac{1}{D_p} \quad (12)$$

D_p is the depletion number and is defined as the ratio of exergy destruction to exergy input of the integrated system [37].

3. Analysis

3.1. Solar Heliostat Field and Pressurized Cavity Receiver

Input and reflected solar radiation to and from the heliostat mirrors are calculated as follows [38]:

$$\dot{Q}_{Solar} = A_h \times N \times DNI \tag{13}$$

$$\dot{Q}_{Heliostats} = \dot{Q}_{Solar} \times \eta_{Opt} \tag{14}$$

where, η_{Opt}, N, and A_h represent the optical efficiency of heliostats, number of heliostats, and aperture area of a single heliostat mirror, number of heliostat mirrors, and aperture area of a single heliostat, respectively.

In this study, conduction heat losses are negligible [39,40]. Heat losses associated with convection and radiation heat transfer from the pressurized cavity receiver are determined by [39]:

$$\dot{Q}_{loss} = \dot{Q}_{loss,conv} + \dot{Q}_{loss,rad} \tag{15}$$

$$\dot{Q}_{loss,conv} = h_{air} A_r (T_{rec,surf} - T_o) \tag{16}$$

$$\dot{Q}_{loss,rad} = \sigma\varepsilon(T_{rec,surf}^4 - T_o^4) \tag{17}$$

where, σ, ε, $T_{rec,surf}$, and A_r represent Stefan-Boltzmann constant, receiver emissivity, receiver surface temperature, and receiver aperture area, respectively. h_{air} is convection heat transfer coefficient which is obtained from [39]:

$$h_{air} = 10.45 - V_a + 10\sqrt{V_a} \tag{18}$$

The heat absorbed by the pressurized air is evaluated from the following equation:

$$\dot{Q}_{abs} = \dot{Q}_{Heliostats} - \dot{Q}_{loss} = \dot{m}(h_{23} - h_{22}) \tag{19}$$

As mentioned earlier, a high temperature latent heat TES medium is utilized to achieve higher efficiency in the unfired gas turbine cycle. The PCM considered here is a eutectic mixture of CaF_2(49)-$CaSO_4$(41.4)-$CaMoO_4$(9.6) with the melting temperature of 943 ℃ [34].

Heat loss during the storage of the PCM unit is considered as 1% [41]. Changes in energy content of the PCM is evaluated by [42,43]:

$$\frac{dE_{PCM}}{dt} = \dot{Q}_{net,PCM} \tag{20}$$

where $\dot{Q}_{net,PCM}$ and E_{PCM} are the heat transfer rate to the PCM and total energy content of PCM, respectively.

Rate of liquefaction/solidification of the PCM is calculated as [42,43]:

$$\frac{dM_{PCM}}{dt} = \frac{\dot{Q}_{net,PCM}}{\Delta h_{melt}} \tag{21}$$

where M_{PCM} and Δh_{melt} represent mass of the liquified PCM and enthalpy of fusion of the eutectic fluoride salt, respectively. Figure 2 shows the variations of direct normal irradiation and wind velocity for the city of Isfahan in central Iran.

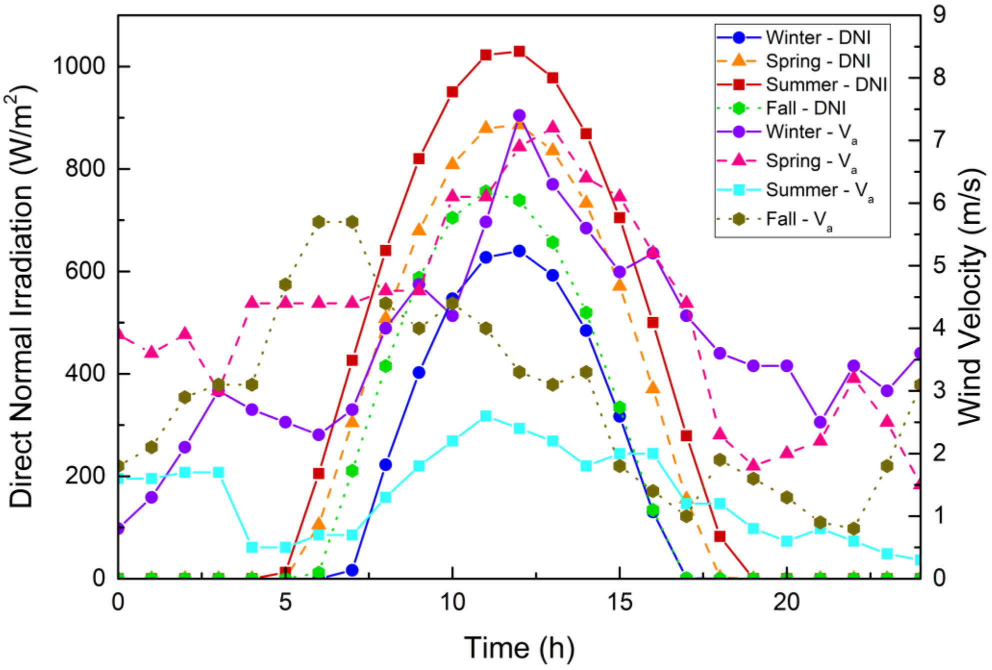

Figure 2 Variations of DNI level and wind velocity for various seasons in Isfahan

3.2 Copper-Chlorine and Rankine Cycles

The specific heat, enthalpy and entropy of various compounds in the Cu-Cl cycle are evaluated as follows [44-47]:

$$C_p^o = A + B \times t + C \times t^2 + D \times t^3 + E/t^2 \quad (22)$$

$$h^o - h_{ref}^o = A \times t + B \times \frac{t^2}{2} + C \times \frac{t^3}{3} + D \times \frac{t^4}{4} - \frac{E}{t} + F - H \quad (23)$$

$$S^o = A \times \ln(t) + B \times t + C \times \frac{t^2}{2} + D \times \frac{t^3}{3} - \frac{E}{2 \times t^2} + G \quad (24)$$

$$t = (\frac{T}{1000}) \quad (25)$$

In the above equations, A-H are the Shomate constants [46]. Rate of thermal energy associated with steam flow and the net power output are calculated as follows:

$$\dot{Q}_{Steam} = \dot{m}_{63}h_{63} + \dot{m}_{41}h_{41} \quad (27)$$

$$\dot{W}_{Net} = \left(\dot{W}_{GT} + \dot{W}_{SRC}\right) - \left(\dot{W}_{AC} + \dot{W}_{Elec} + \dot{W}_P\right) \quad (28)$$

Here, subscripts *p, SRC, GT*, *AC*, and *Elec* denote pump, steam Rankine cycle, gas turbine, air compressor, and electrolyzer, respectively. Integrated system overall energy and exergy efficiencies are expressed as:

$$\eta_I = (\dot{n}_{H_2}LHV_{H_2} + \dot{W}_{Net} + \dot{Q}_{Steam})/\dot{Q}_{Solar} \quad (29)$$

$$\eta_{II} = 1 - (\dot{E}x_{d,total}/\dot{E}x_{Solar}) \quad (30)$$

Input data and assumptions for the base case study are listed in Table 1 [34,48-52].

Table 1 Input data and assumptions of various subsystems for the base case study

Subsystem	Parameter	Value

Solar Heliostat Field	Optical efficiency (%)	75
	Number of heliostats	5,000
	Aperture area of each heliostat (m^2)	11×11
Pressurized Cavity Receiver	Receiver aperture area (m^2)	60
	Average surface temperature of the receiver (℃)	1,100
	Receiver emissivity (%)	88
Unfired gas turbine cycle	Pressure ratio	8.2
	Air compressor isentropic efficiency (%)	80
	Gas turbine isentropic efficiency (%)	86
	Temperature of air entering the turbine (℃)	943
PCM unit	Melting temperature (℃)	943
	Enthalpy of fusion (kJ/kg)	237
	Temperature of air entering the CuCl cycle (℃)	600
Cu-Cl cycle	Temperature of hydrolysis step (℃)	400
	Temperature of thermolysis step (℃)	530
	Temperature of electrolysis step (℃)	25
	Temperature of drying step (℃)	70
Steam Rankine cycle	Condenser pressure (kPa)	10
	First bleed pressure of steam turbine (kPa)	2,500
	Second bleed pressure of steam turbine (kPa)	1,500
	Boiler pressure (kPa)	15,000
	Turbine inlet temperature (℃)	400
	Steam turbine isentropic efficiency (%)	86

Pumps isentropic efficiency (%)	80

4. Results and Discussion

4.1. Validation

The results for the Cu-Cl cycle are compared with those presented by previous studies [53] and [54]. For heat exchanger effectiveness of 75%, and 100%, the results of current model are presented and compared with previous studies in Fig. 3. As can be seen, the results are in good agreement with past reported studies.

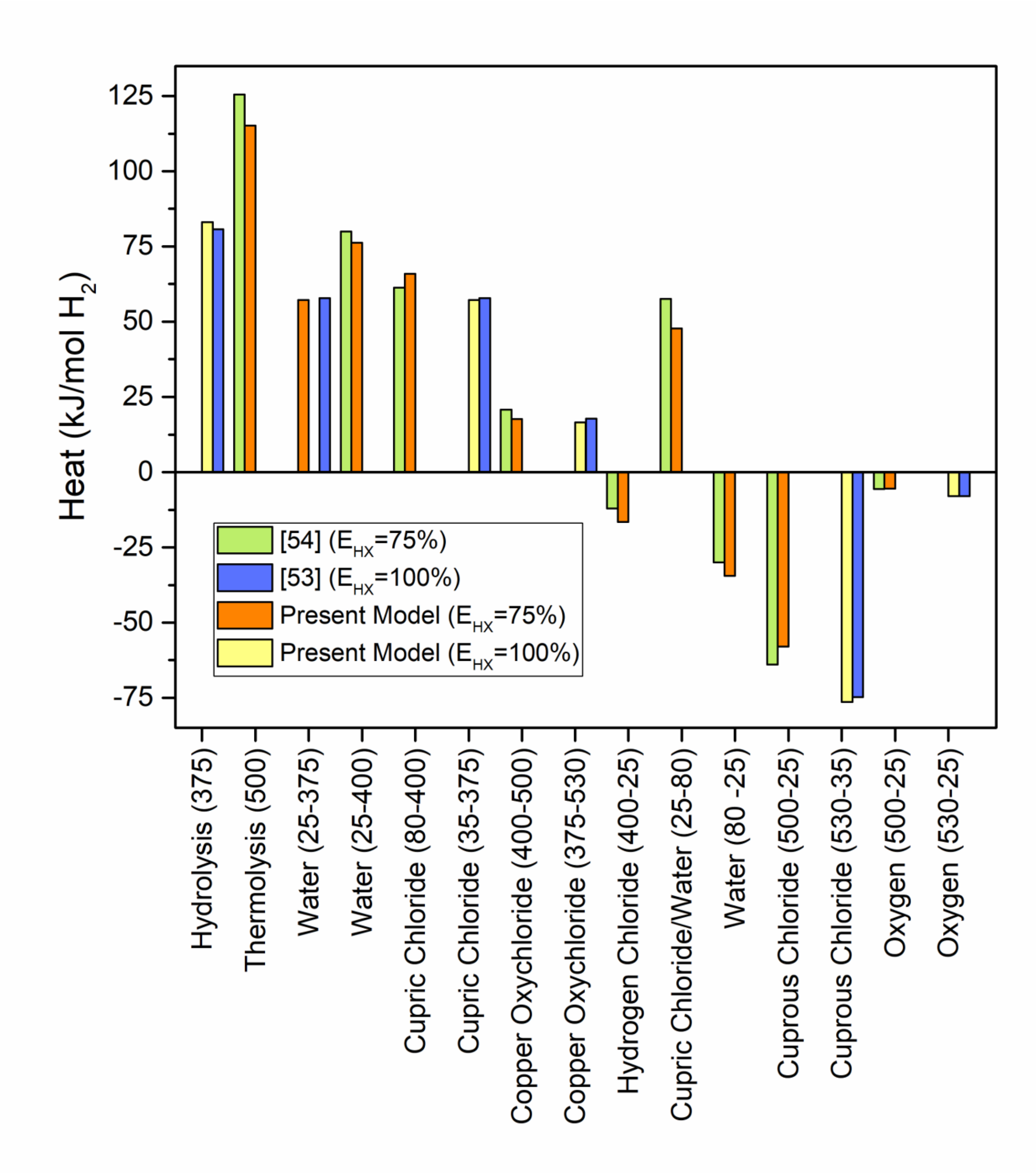

Figure 3 A comparison between the results for the Cu-Cl cycle with past studies

The main results for the integrated system are shown in Table 2. The overall energy and exergy efficiencies of the integrated system are obtained as 49.9% and 44.9%, respectively. For the base case, electricity, hydrogen, oxygen, and steam are produced at the rates of 41.9 MW, 0.19 kg/s, 0.76 kg/s, and 12.6 kg/s, respectively. The sustainability index of the plant is obtained as 1.81.

Table 2 Main results of the integrated energy system for the base case study

Parameter	Value
Overall energy efficiency (%)	49.9
Overall exergy efficiency (%)	44.9
Amount of produced hydrogen (kg/s)	0.19
Amount of produced oxygen (kg/s)	0.76
Net generated electricity (MW)	41.9
Produced steam (kg/s)	12.6
Total exergy destruction (MW)	111
Sustainability index	1.81

The Sankey diagram shown in Fig. 4 presents the exergy destruction of various subsystems and components of the integrated system. As can be seen, 37.8% of the input exergy which is equal to 76.5 MW is destroyed in the solar heliostat field and the receiver. The exergy destruction rates associated with Cu-Cl cycle, Rankine cycle, and heat recovery units are 4.4%, 3.25%, and 2.5% of the total exergy input, respectively. Advantage of Sankey diagram is in improving the sustainability of the proposed energy plant. The exergy destruction of different components shows the prioritization for the next advancement in the energy plant. Additionally, it can be used to identify the large sources of system irreversibility. This way it is possible to focus on each source and reduce the deficiencies in energy system performance by selecting right input parameters or refining the overall design in future studies.

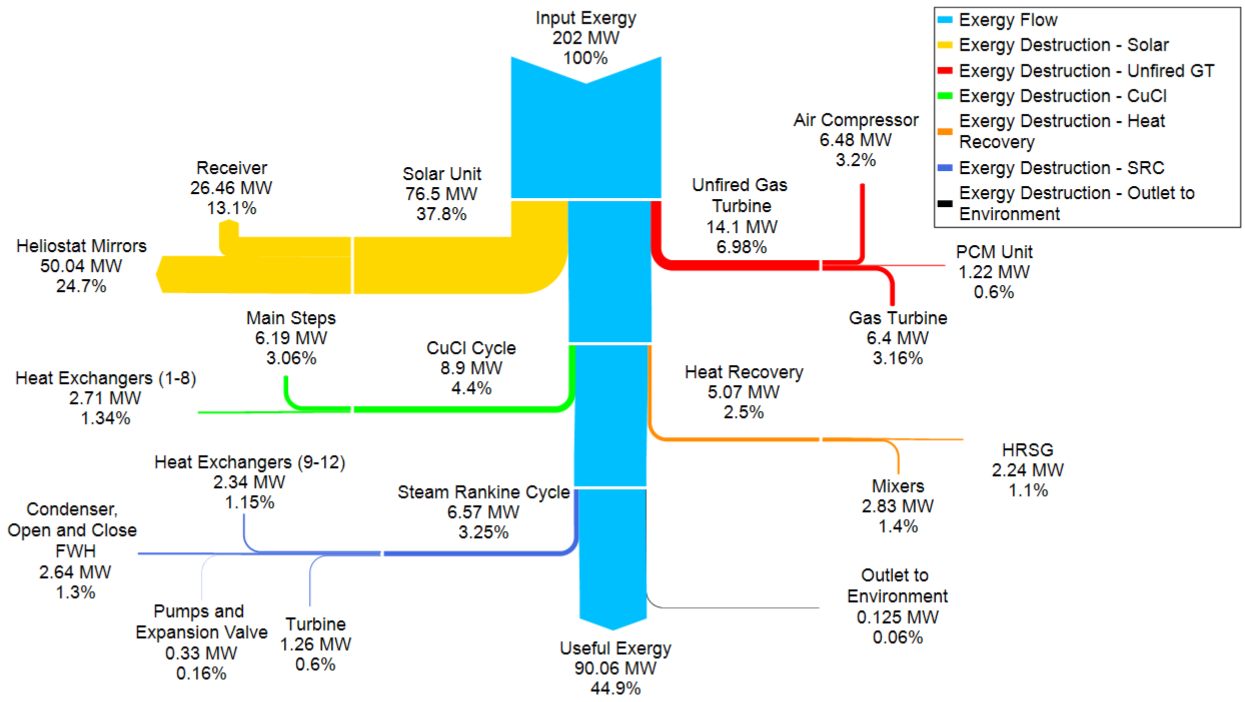

Figure 4 Sankey diagram for the exergy flow and exergy destruction of the integrated energy system

Variations of solar input heat and heat losses for different seasons are shown in Fig. 5. The maximum heat input from the heliostat mirrors ranges from 387 MW in winter to over 623 MW in summer. Additionally, heat losses associated with solar heliostat field and pressurized cavity receiver increase from 101 MW in winter to 159 MW in summer which indicates a 57% increase in the heat losses.

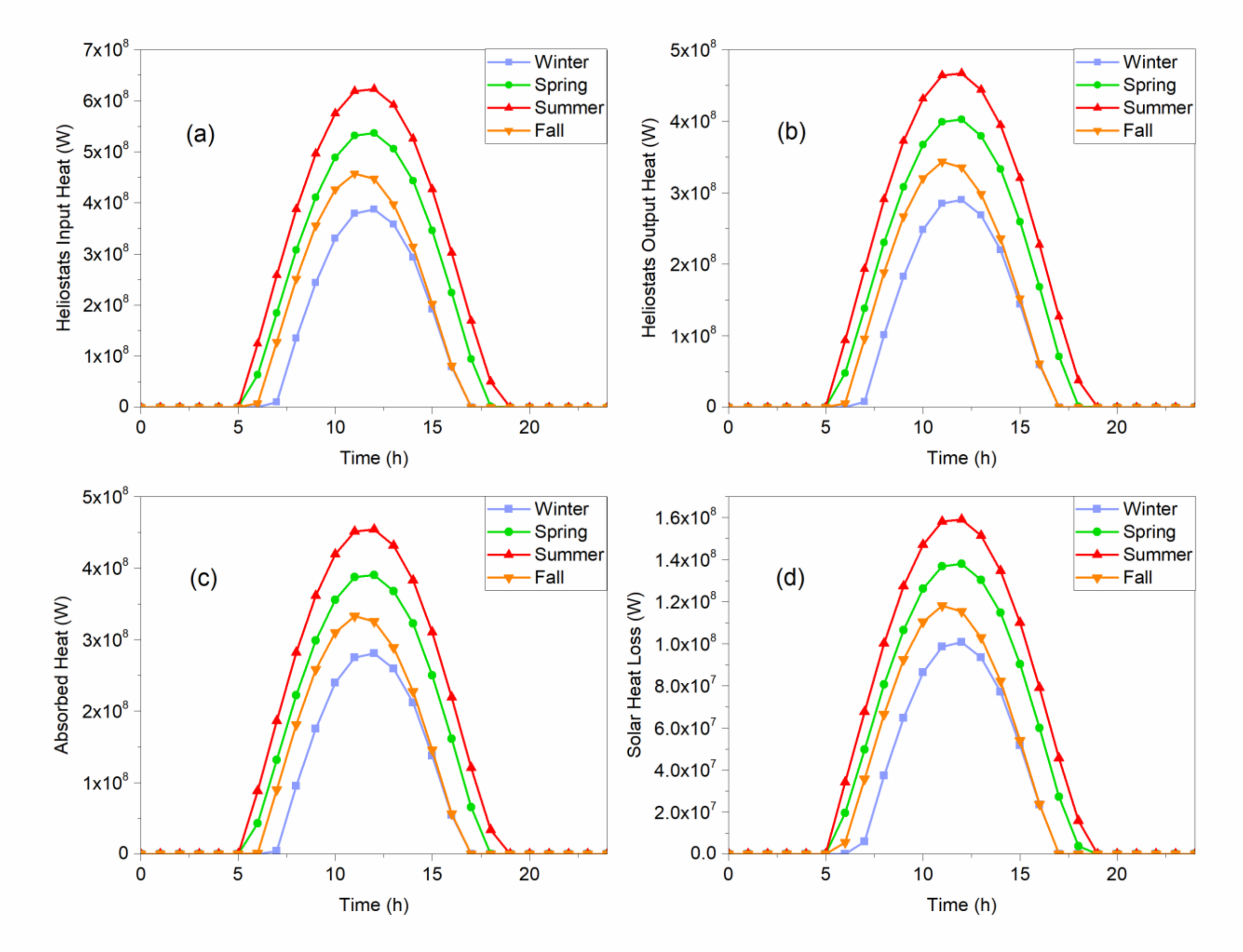

Figure 5 Performance of solar power tower system in different seasons: (a) heliostats input heat, (b) heliostats output heat, (c) absorbed heat by air, and (d) overall solar heat losses

Effects of various input parameters on the overall integrated system performance are investigated in this paper. The effect of the number of heliostat mirrors on the overall integrated system performance is shown in Fig. 6. Ascan be seen, net power output, hydrogen production rate, and exergy destruction increase linearly with an increase in the heliostat numbers. As the number of heliostat mirrors increase from 3,000 to 6,000, the hydrogen production rate and net power output increase from 0.11 kg/s and 24.94 MW to 0.27 kg/s and 58.90 MW, respectively.

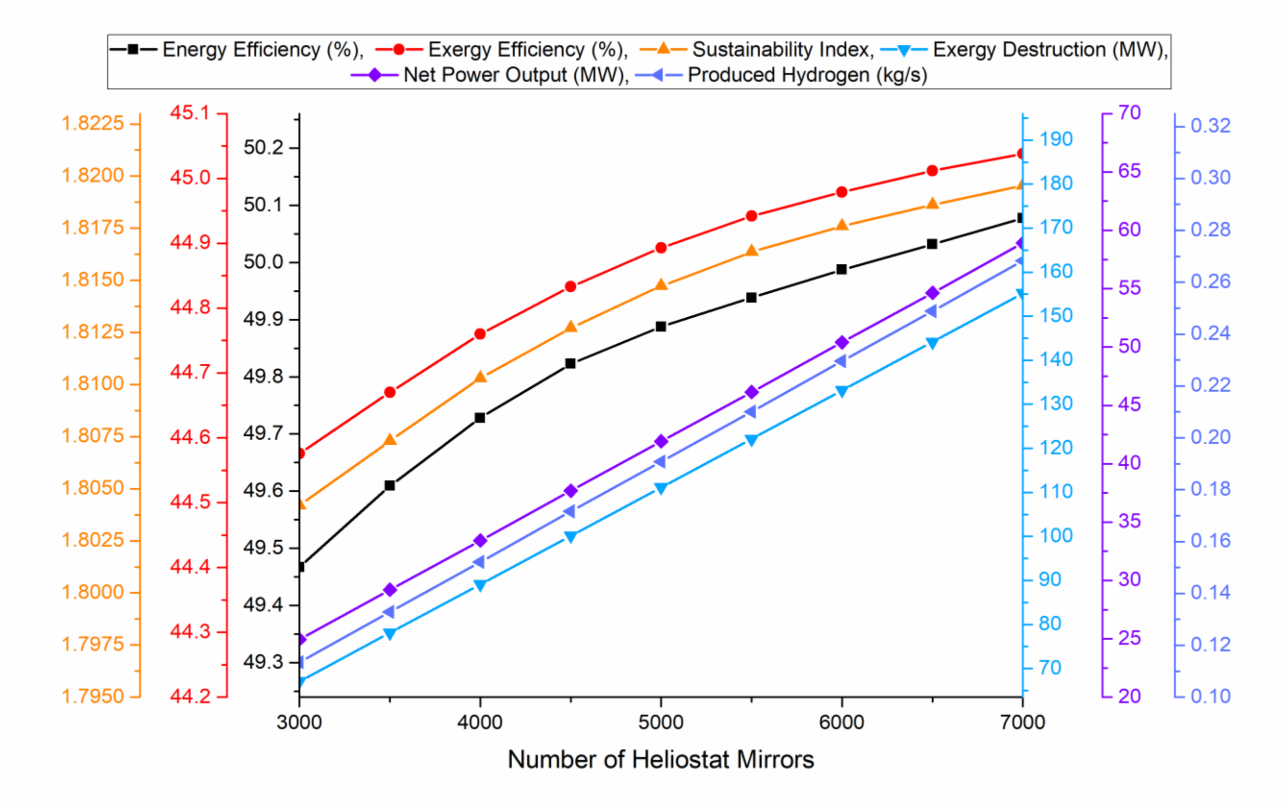

Figure 6 Influence of the number of heliostat mirrors on the overall integrated system performance

The effect of the gas turbine pressure ratio on the overall integrated system performance are shown in Fig. 7. Maximum power output and overall energy efficiency occur at pressure ratios of around 6-8. However, at these pressure ratios, the rate of hydrogen production is minimized.

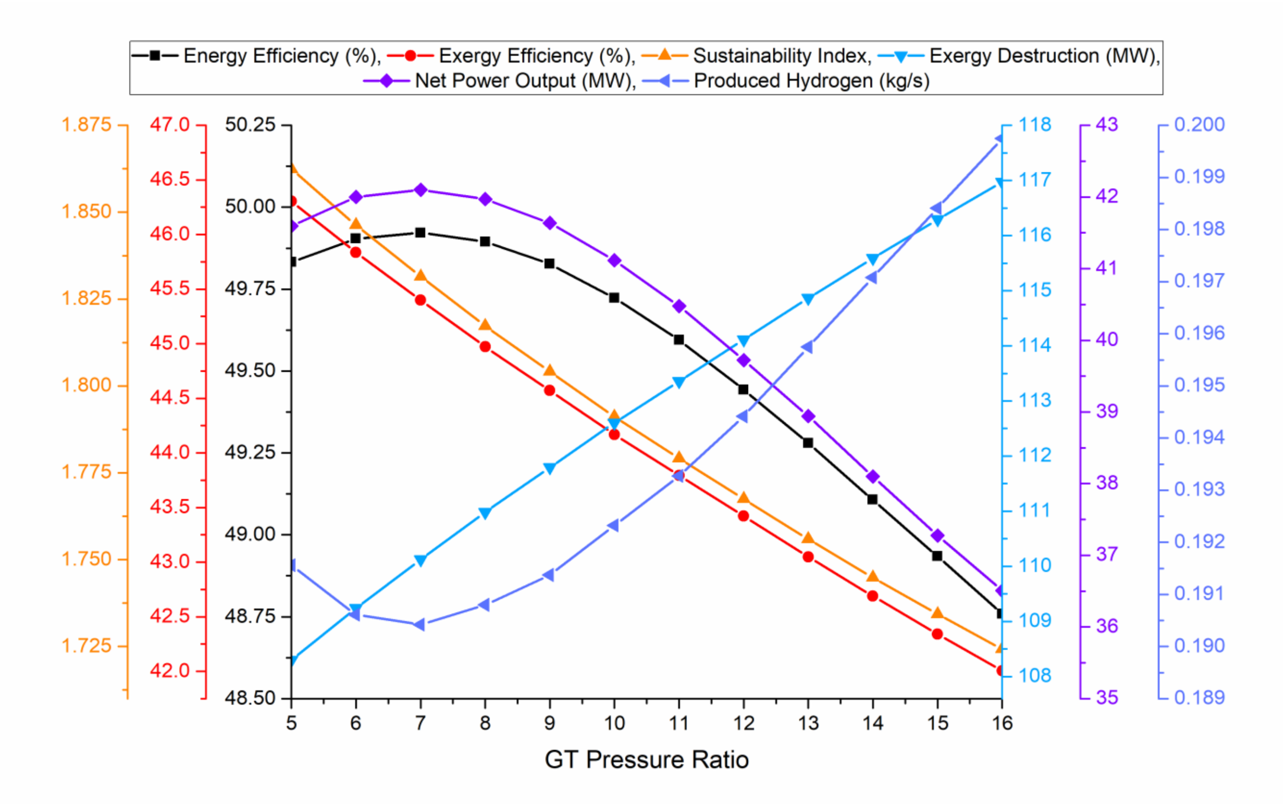

Figure 7 Influence of gas turbine pressure ratio on the overall integrated system performance

The influence of the inlet hot air temperature to the Cu-Cl cycle (T_{26}) on the overall integrated system performance is shown in Fig. 8. As it can be seen, by increasing the temperature of this state in the second phase of heating the hot air, higher amount of energy will be discharged from the PCM tank and therefore, the mass flow rate of air which enters the air compressor is reduced and hence all of the integrated system outputs are reduced. There is one exception and that is the molar flow rate of produced hydrogen which is directly related to the temperature of state 26. Because the temperature difference between state 26 and state 27 is quite low (less than 100 ℃ for the base case); whenever the temperature of state 26 increases the flow rate of air entering the thermolysis reactor reduces and therefore, more air is left to run the Cu-Cl cycle and produce higher amount of hydrogen.

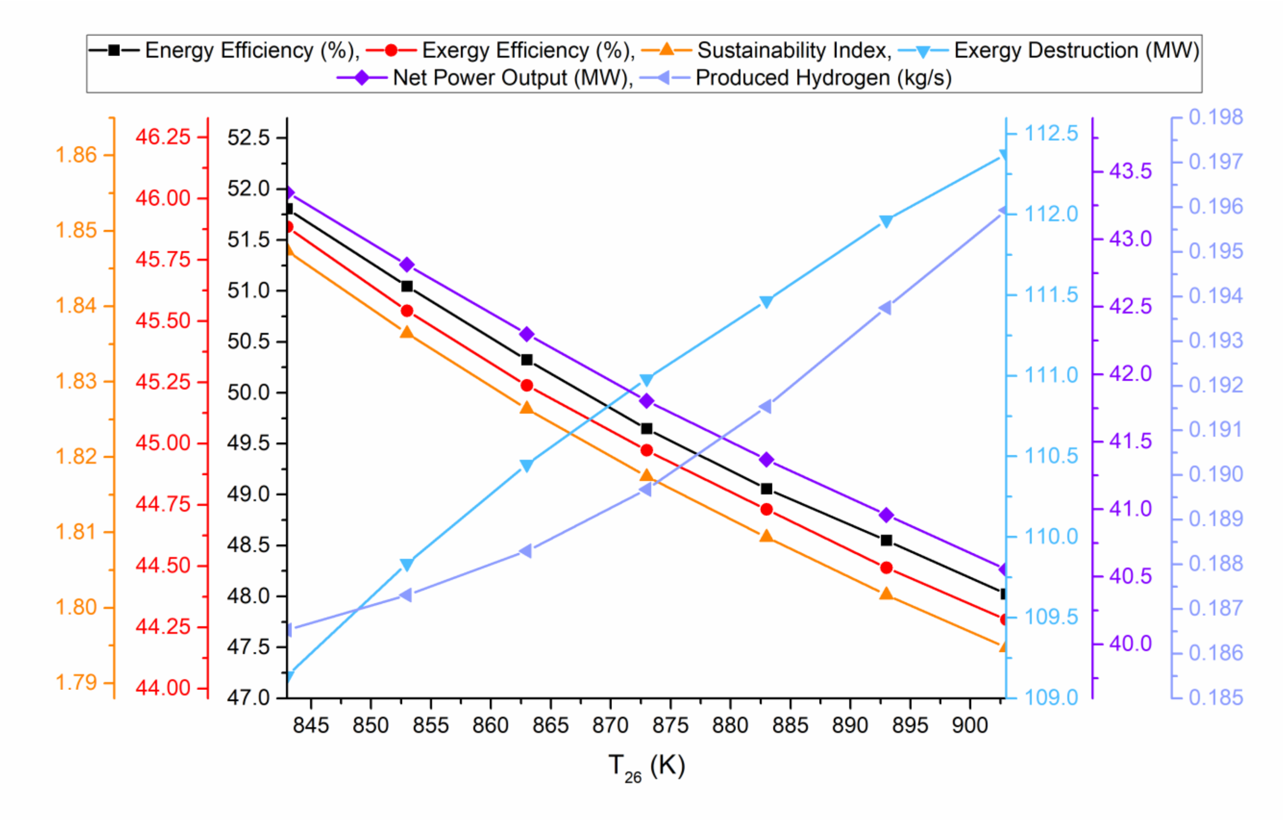

Figure 8 Influence of T_{26} on the overall integrated system performance

Figure 9 shows the effect of variations in the hydrolysis temperature on the overall integrated system performance. As it is observable, by increasing the hydrolysis reaction temperature, more air has to flows through the hydrolysis reactor which causes a decrease in the net power output and the hydrogen production rate of the energy system. However, energy and exergy efficiencies of the integrated system increase due to an increase in the steam production rate.

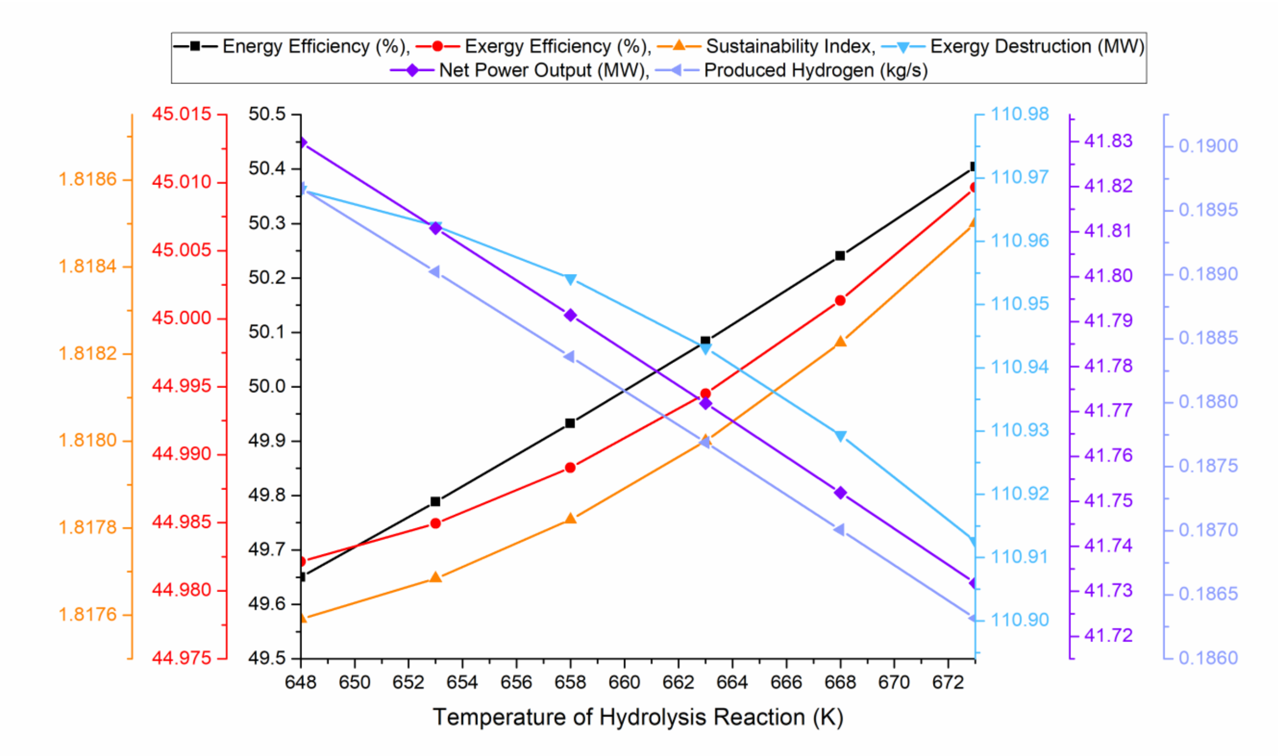

Figure 9 Influence of hydrolysis reaction temperature on the overall integrated system performance

As shown in Fig. 10, by increasing the thermolysis reaction temperature, net power output, and rate of produced hydrogen increase. This causes an improvement in the energy and exergy efficiencies of the integrated system. It is noted that if the integrated system did not include a heat recovery steam generator unit, an increase in the thermolysis reaction temperature would reduce the energy system performance.

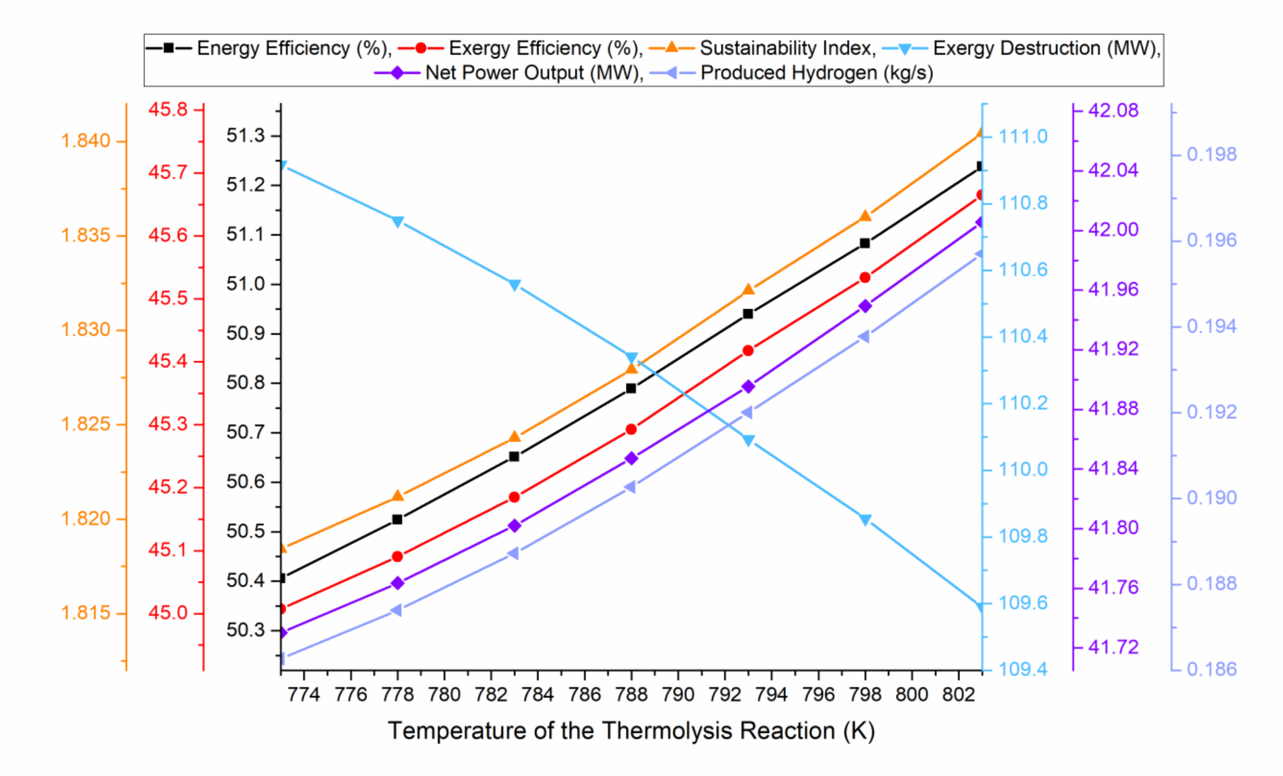

Figure 10 Influence of thermolysis reaction temperature on overall integrated system performance and output

The results for the novel integrated system proposed in this paper are compared with those for other solar-based hydrogen production systems investigated in past studies. As shown in Fig. 11, the present energy system has the highest overall energy efficiency among other systems. This is mainly because of the heat recovery unit included in the integrated system. Also, despite relatively high exergy destructions in the heat recovery unit and the gas turbine cycle, the overall exergy efficiency of the proposed energy system is desirable.

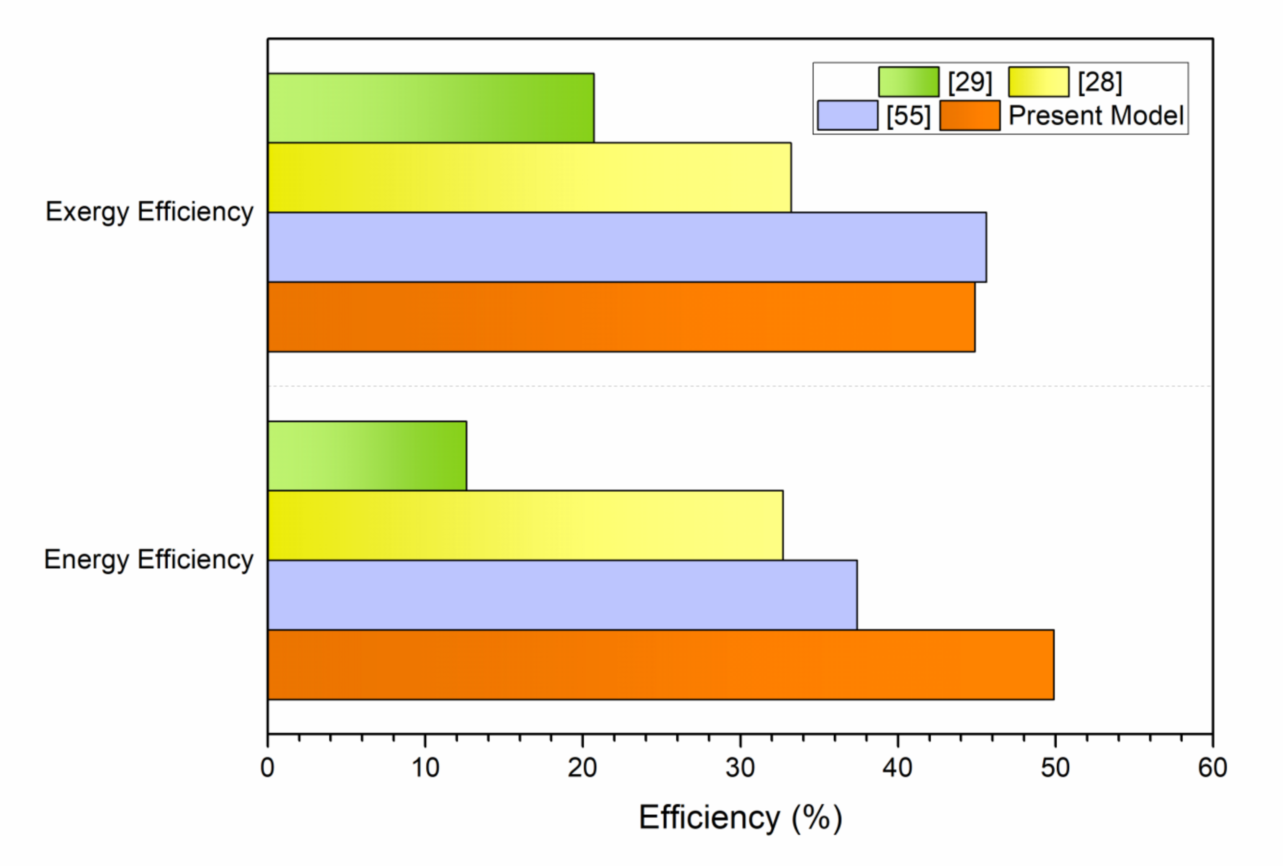

Figure 11 Comparison between the overall efficiency of the proposed integrated system and other solar systems

5. Conclusions

A novel solar powered integrated system for the production of thermochemical hydrogen, oxygen, power, and steam for heating purposes is analysed in this study. The proposed integrated system utilizes a solar power tower with pressurized cavity receiver, unfired gas turbine cycle with PCM thermal energy storage, four-step Cu-Cl cycle, regenerative steam Rankine cycle, and heat recovery unit. The impact of the thermal energy storage on the hydrogen production cycle can be concluded as:

- Overall integrated system energy and exergy efficiencies are 49.9% and 44.9%, respectively.
- For the baseline of this study, 0.19 kg/s of hydrogen, 0.76 kg/s of oxygen, 41.9 MW of electricity, and 12.6 kg/s of steam are produced.

- Heat losses associated with solar heliostat field and pressurized cavity receiver increases over 57% from 101 MW in winter to 159 MW in summer.
- Highest exergy destructions occur in the solar power tower system and unfired gas turbine cycle which consume 37.8% and 6.98% of the overall integrated system exergy input.

Influences of various input parameters, including the number of heliostats, pressure ratio of the gas turbine, air inlet temperature to the Cu-Cl cycle, hydrolysis reaction temperature, and thermolysis reaction temperature on the overall energy system performance are investigated. It was concluded that by increasing the number of heliostats mirrors from 3,000 to 6,000, it is possible to increase the power generation of the cycle by 33.96 MW. Additionally, investigation on the influence of gas turbine pressure ratio on system performance showed that the energy efficiency, and power generation of the cycle is maximized at the pressure ratio of 7. Our results indicated that by increasing the temperature of hydrolysis and thermolysis reactions, both energy and exergy efficiencies will be increased.

A comparison between the proposed integrated and other solar systems studied in the past shows the proposed integrated system has the highest performance compared to previous solar hydrogen systems in terms of energy and exergy efficiencies.

References

1. International Energy Agency, World Energy Balances: Overview, IEA, Paris. Available online at: https://www.iea.org/reports/world-energy-balances-overview; [accessed 05.08.2020].
2. Owusu, P. A., Asumadu-Sarkodie, S. A review of renewable energy sources, sustainability issues and climate change mitigation. Cogent Engineering, 3(1), 1167990, 2016.

3. Palmer, G., Floyd, J. Energy Storage and Civilization: A Systems Approach (Vol. 40). Springer Nature, 2020.
4. Mohammadi, K., Khanmohammadi, S., Khorasanizadeh, H., Powell, K. A comprehensive review of solar only and hybrid solar driven multigeneration systems: Classifications, benefits, design and prospective. Applied Energy, 268, 114940, 2020.
5. Ahmadi, P., Khanmohammadi, S., Musharavati, F., Afrand, M. Development, evaluation, and multi-objective optimization of a multi-effect desalination unit integrated with a gas turbine plant. Applied Thermal Engineering, 115414, 2020.
6. Sahoo, U., Kumar, R., Singh, S. K., Tripathi, A. K. Energy, exergy, economic analysis and optimization of polygeneration hybrid solar-biomass system. Applied Thermal Engineering, 145, 685-692, 2018.
7. Li, Y., Liu, Y. Oxygen enrichment and its application to life support systems for workers in high-altitude areas. International journal of occupational and environmental health, 20(3), 207-214, 2014.
8. Sun, W., Wang, Q., Zhou, Y., Wu, J. Material and energy flows of the iron and steel industry: Status quo, challenges and perspectives. Applied Energy, 268, 114946, 2020.
9. Dutta, S. A review on production, storage of hydrogen and its utilization as an energy resource. Journal of Industrial and Engineering Chemistry, 20(4), 1148-1156, 2014.
10. Sadeghi, S., Ghandehariun, S., Rosen, M. A. Comparative economic and life cycle assessment of solar-based hydrogen production for oil and gas industries. Energy, 118347, 2020.
11. Kalamaras, C. M., Efstathiou, A. M. Hydrogen production technologies: current state and future developments. In Conference papers in energy, Vol. 2013. Hindawi, 2013.
12. Bhosale, R. R., Kumar, A., Sutar, P. Thermodynamic analysis of solar driven SnO2/SnO based thermochemical water splitting cycle. Energy Conversion and Management, 135, 226-235, 2017.

13. Muhich, C. L., Ehrhart, B. D., Al-Shankiti, I., Ward, B. J., Musgrave, C. B., Weimer, A. W. A review and perspective of efficient hydrogen generation via solar thermal water splitting. Wiley Interdisciplinary Reviews: Energy and Environment, 5(3), 261-287, 2016.
14. Kumar, S. S., Himabindu, V. Hydrogen production by PEM water electrolysis–A review. Materials Science for Energy Technologies, 2(3), 442-454, 2019.
15. Lu, Y., Zhu, L., Agrafiotis, C., Vieten, J., Roeb, M., Sattler, C. Solar fuels production: two-step thermochemical cycles with cerium-based oxides. Progress in Energy and Combustion Science, 75, 100785, 2019.
16. Ji, G., Yao, J.G., Clough, P.T., Da Costa, J.C.D., Anthony, E.J., Fennell, P.S., Wang, W., Zhao, M. Enhanced hydrogen production from thermochemical processes. Energy & Environmental Science, 11(10), pp.2647-2672, 2018.
17. Acar, C., Dincer, I. Review and evaluation of hydrogen production options for better environment. Journal of Cleaner Production, 218, 835-849, 2019.
18. Park, J., Lee, S. Y., Lee, I. B. Study of alternative reactor–separator network in bunsen process of sulfur-iodine cycle for hydrogen production. Journal of Chemical Engineering of Japan, 52(7), 638-649, 2019.
19. Manan, S.S., Jianu, O.A., Rosen, M.A. Investigation of Heat Extraction Methods from Cuprous Chloride for Improving the Efficiency of the Thermochemical Copper-Chlorine Cycle. European Journal of Sustainable Development Research, 3(1), em0075, 2019.
20. Wang, Z. L., Naterer, G. F., Gabriel, K. S., Gravelsins, R., Daggupati, V. N. Comparison of sulfur–iodine and copper–chlorine thermochemical hydrogen production cycles. International Journal of Hydrogen Energy, 35(10), 4820-4830, 2010.
21. Avsec, J., Wang, Z., Naterer, G. F. Thermodynamic and transport properties of fluids and solids in a Cu–Cl solar hydrogen cycle. Journal of Thermal Analysis and Calorimetry, 127(1), 961-967, 2017.

22. Achkari, O., El Fadar, A. Latest developments on TES and CSP technologies–Energy and environmental issues, applications and research trends. Applied Thermal Engineering, 167, 114806, 2020.

23. Pelay, U., Luo, L., Fan, Y., Stitou, D., Rood, M. Thermal energy storage systems for concentrated solar power plants. Renewable and Sustainable Energy Reviews, 79, 82-100, 2017.

24. Rezaie, B., Reddy, B. V., Rosen, M. A. Thermodynamic analysis and the design of sensible thermal energy storages. International Journal of Energy Research, 41(1), 39-48, 2017.

25. Mofijur, M., Mahlia, T.M.I., Silitonga, A.S., Ong, H.C., Silakhori, M., Hasan, M.H., Putra, N., Rahman, S.M. Phase change materials (PCM) for solar energy usages and storage: an overview. Energies, 12(16), p.3167, 2019.

26. Ghandehariun, S., Naterer, G. F., Dincer, I., Rosen, M. A. Solar thermochemical plant analysis for hydrogen production with the copper–chlorine cycle. International Journal of Hydrogen Energy, 35(16), 8511-8520, 2010.

27. Ouagued, M., Khellaf, A., Loukarfi, L. Performance analyses of Cu–Cl hydrogen production integrated solar parabolic trough collector system under Algerian climate. International Journal of Hydrogen Energy, 43(6), 3451-3465, 2018.

28. Ishaq, H., Dincer, I. A comparative evaluation of OTEC, solar and wind energy based systems for clean hydrogen production. Journal of Cleaner Production, 246, 118736, 2020.

29. Al-Zareer, M., Dincer, I., Rosen, M. A. Development and assessment of a new solar heliostat field based system using a thermochemical water decomposition cycle integrated with hydrogen compression. Solar Energy, 151, 186-201, 2017.

30. Yilmaz, F. Thermodynamic performance evaluation of a novel solar energy based multigeneration system. Applied Thermal Engineering, 143, 429-437, 2018.

31. Yilmaz, F., Ozturk, M., Selbas, R. Energy and exergy performance assessment of a novel solar-based integrated system with hydrogen production. International Journal of Hydrogen Energy, 44(34), 18732-18743, 2019.

32. Ishaq, H., Dincer, I. Design and performance evaluation of a new biomass and solar based combined system with thermochemical hydrogen production. Energy conversion and management, 196, 395-409, 2019.

33. Awad, A., Burns, A., Waleed, M., Al-Yasiri, M., Wen, D. Latent and sensible energy storage enhancement of nano-nitrate molten salt. Solar Energy, 172, 191-197, 2018.

34. Sadeghi, S., Ghandehariun, S. Thermodynamic analysis and optimization of an integrated solar thermochemical hydrogen production system. In Press, International Journal of Hydrogen Energy, 2020.

35. Ghandehariun, S., Rosen, M. A., Naterer, G. F. Direct contact heat transfer from molten salt droplets in a thermochemical water splitting process of hydrogen production. International Journal of Heat and Mass Transfer, 96, 125-131, 2016.

36. Moran, M. J. Engineering thermodynamics: fundamentals. CRC Handbook of Thermal Engineering,, 3-14, 2017.

37. Rosen, M. A., Dincer, I., Kanoglu, M. Role of exergy in increasing efficiency and sustainability and reducing environmental impact. Energy policy, 36(1), 128-137, 2008.

38. Habibi, H., Zoghi, M., Chitsaz, A., Javaherdeh, K., Ayazpour, M., Bellos, E. Working fluid selection for regenerative supercritical Brayton cycle combined with bottoming ORC driven by molten salt solar power tower using energy–exergy analysis. Sustainable Energy Technologies and Assessments, 39, 100699, 2020.

39. Meriche, I. E., Beghidja, A., Boumedjirek, M. Energetic and exergetic analysis of solar gas turbine power plant in South Algeria. In 2014 5th International Renewable Energy Congress (IREC), pp. 1-6. IEEE, 2014.

40. Xu, C., Wang, Z., Li, X., Sun, F. Energy and exergy analysis of solar power tower plants. Applied Thermal Engineering, 31(17-18), 3904-3913, 2011.
41. Gómez-Hernández, J., González-Gómez, P. A., Briongos, J. V., Santana, D. Influence of the steam generator on the exergetic and exergoeconomic analysis of solar tower plants. Energy, 145, 313-328, 2018.
42. Dincer, I., Rosen, M. Thermal energy storage: systems and applications, Second Edition, John Wiley & Sons, 2010.
43. Garg, H. P., Mullick, S. C., Bhargava, V. K. Solar thermal energy storage. Springer Science & Business Media, 2012.
44. National Institute of Standards and Technology (NIST), http://webbook.nist.gov/chemistry/form-ser.html; 2020 [accessed 20.01.2020]
45. The Exergoecology Portal, http://www.exergoecology.com/excalc/; [accessed 20.01.2020].
46. Balta, M. T., Dincer, I., Hepbasli, A. Exergoeconomic analysis of a hybrid copper–chlorine cycle driven by geothermal energy for hydrogen production. International Journal of Hydrogen Energy, 36(17), 11300-11308, 2011.
47. Yılmaz, F., Balta, M. T. Energy and exergy analyses of hydrogen production step in boron based thermochemical cycle for hydrogen production. International Journal of Hydrogen Energy, 42(4), 2485-2491, 2017.
48. Ishaq, H., Dincer, I., Naterer, G. F. New trigeneration system integrated with desalination and industrial waste heat recovery for hydrogen production. Applied Thermal Engineering, 142, 767-778, 2018.
49. Sadeghi, S., Ghandehariun, S., Naterer, G. F. Exergoeconomic and Multi-objective Optimization of a Solar Thermochemical Hydrogen Production Plant with Heat Recovery. 2020.

50. Li, X., Kong, W., Wang, Z., Chang, C., & Bai, F. Thermal model and thermodynamic performance of molten salt cavity receiver. Renewable energy, 35(5), 981-988, 2010.

51. Ghandehariun, S., Rosen, M.A., Naterer, G.F. Thermal efficiency improvement of hydrogen production via thermochemical water splitting" IEEE International Conference on Smart Energy Grid Engineering (SEGE'13), Oshawa, ON, August 28-30, 2013.

52. Zhou, C., Wu, S. Medium-and high-temperature latent heat thermal energy storage: Material database, system review, and corrosivity assessment. International Journal of Energy Research, 43(2), 621-661, 2019.

53. Ghandehariun, S., Naterer, G.F., Rosen, M.A. Rosen, Wang, Z. Pinch analysis for recycling thermal energy in the Cu-Cl cycle", International Journal of Hydrogen Energy, vol. 37, pp. 16535-16541, 2012.

54. Orhan, M. F., Dinçer, İ., Rosen, M. A. Efficiency comparison of various design schemes for copper–chlorine (Cu–Cl) hydrogen production processes using Aspen Plus software. Energy Conversion and Management, 63, 70-86, 2012.

55. Ratlamwala, T. A. H., Dincer, I. Comparative energy and exergy analyses of two solar-based integrated hydrogen production systems. International Journal of Hydrogen Energy, 40(24), 7568-7578, 2015.